Finite contact duration modeling of a Vibro-Impact Nonlinear Energy Sink to protect a civil engineering frame structure against seismic events

Stefania Lo Feudo, Stéphane Job, Miriam Cavallo, Aguinaldo Fraddosio, Mario Daniele Piccioni, Alessandro Tafuni

Finite contact duration modeling of a Vibro-Impact Nonlinear Energy Sink to protect a civil engineering frame structure against seismic events

S. Lo Feudo[a,*], S. Job[a], M. Cavallo[b,a], A. Fraddosio[b], M.D. Piccioni[b], A. Tafuni[b,a]

[a] *QUARTZ, ISAE-Supméca, 3 Rue Fernand Hainaut, 93400 Saint-Ouen-sur-Seine, France*
[b] *Polytechnic University of Bari, 4 Via Edoardo Orabona, 70126 Bari, Italy*

Abstract

This paper reassesses carefully the effects and consequences of instantaneous contact mechanics versus finite contact duration modeling of Vibro-Impact Nonlinear Energy Sinks (VI NES). The device is composed of a container enclosing an inelastic sphere, interacting via a nonlinear viscoelastic dissipative force with the inner walls of the container. The VI NES is considered in a practical context, the control of the vibrations of a civil engineering frame structure under seismic input. It is connected by a rigid link to the structure: the particle bounces within the container when it vibrates, exploring dynamical regimes ranging from periodic collisions to chaos while dissipating energy. Our VI NES is designed in order to mitigate vibrations of a ten-story frame structure under two historic earthquake signals, in order to rule out specific effects. The dynamics of the system, obtained from both finite and instantaneous contact models, are compared and discussed. The main result reveals a significant effect of the contact duration on the estimation of the dissipated energy, even for very brief collisions. Instantaneous contact model indeed provides incommensurate values in terms of acceleration during the impacts, leading to a higher sensitivity to Initial Conditions (IC) revealed by large fluctuations of the mechanical response. In turn, any finite duration contact models is proved to be less sensitive to IC, and thus more precise. Our findings demonstrate that both finite and instantaneous models converge in fact to the same value, in average, but the finite duration models require much less realizations to converge to the mean value. In practice, the finite contact duration low pass filters the mechanical responses of the VI NES, avoiding the system to fall into nonphysical chaotic states experienced by the instantaneous model.

Keywords: Vibro-impact damper, Nonlinear Energy Sink, contact mechanics, passive control, earthquake engineering

*Corresponding author

Email addresses: stefania.lofeudo@isae-supmeca.fr (S. Lo Feudo), stephane.job@isae-supmeca.fr (S. Job), m.cavallo4@studenti.poliba.it, miriam.cavallo@edu.supmeca.fr (M. Cavallo), aguinaldo.fraddosio@poliba.it (A. Fraddosio),

1. Introduction

Dynamic responses of structures due to wind load and seismic excitation still remain a major concern in the field of civil engineering. In particular, during its life-cycle, a building can undergo several seismic events, which may affect the integrity of structural elements and change its overall dynamic properties. Even during one earthquake, if particularly severe, the structure might suffer for damages capable of substantially changing its vibration features [1–3]. Also, the stiffening effect of filling walls is generally not considered in seismic design: the brittle behavior of filling walls might lead to a sudden and significant decrease of the stiffness during an earthquake [4–6].

In this frame, a promising technology for passive vibrations control are Nonlinear Energy Sinks (NES), which are essentially nonlinear oscillators, i.e. oscillators without linear restoring force. Since a NES has no inherent eigenfrequency, it can in principle tune to any resonant frequency of the primary structure, by giving rise to an irreversible energy transfer from the main system to the NES above a certain excitation threshold, [7–10]. Previous studies have shown that this threshold increases with frequency, such that a NES may require the reception of high input energy to start vibrating and activating the Targeted Energy Transfer (TET). This drawback reduces the effectiveness of NES in a Multi-Degrees Of Freedom (MDOF) system [11, 12]. However, specific NESs designs may lead to bistability, and thus to a broadband quasi-periodic or chaotic oscillations. According to Refs. [11, 13] this improves indeed the absorption of vibrations and reduces the minimal energy threshold for activating the TET.

From the technological point of view, a NES can be obtained, for example, by a mass moving transversely in a nonlinear potential [14–17], by magnetic forces [12, 18, 19], by coupling a rotating mass with a primary structure [20], by a mass sliding on a curved track [21] and by vibro-impact systems [22]. Configurations of vibro-impact systems include rotary NESs [23], track NESs [24] and vibro-impact NESs. In regard to the latter, one refers to single-sided vibro-impact NES [25, 26] or double-sided vibro-impact NES [27, 28] depending on the number of barriers added along the trajectory of the moving mass. Notably, Ref. [29] has proven that symmetry breaking due to the use of one or multiple single-sided vibro-impact dampers makes energy dissipation less dependent on the size of the system.

Some studies focused on the case of impacting barriers connected to the primary structure by linear springs [30–32]. Bumpers were also modeled as linear springs-dashpots in [33, 34], and either linear or nonlinear springs in [35]. More precisely, piecewise NESs addressed by Ref. [35] are equipped with continuous linear damping and nonlinear spring with negative stiffness.

The present paper deals with a Vibro-Impact Nonlinear Energy Sink (VI NES) damper rigidly linked to the primary structure as in [36–38]. The device is composed of a hollow rigid container hosting a deformable spherical particle. When the rigid box connected to the primary structure oscillates, the inner particle bounces and impacts against the edges,

mariodaniele.piccioni@poliba.it (M.D. Piccioni), a.tafuni2@studenti.poliba.it, alessandro.tafuni@edu.supmeca.fr (A. Tafuni)

thereby dissipating energy. We consider this design since we are interested in exploring the dissipation coming from collisions instead of modal interactions. Compared to previous designs involving dissipative elastic stops, as in [35], the damping force is not continuous here and arises only during collisions.

Performance of one or more VI NES on a two degrees of freedom primary system under seismic excitation was addressed in Ref. [39]. The authors underlined that the VI NES has two beneficial effects on seismic mitigation. Firstly, TET takes place at the initial stage of the ground motion, when the primary structure is highly stressed. Secondly, the VI NES redistributes energy to higher frequencies. The clearance of the VI NES, that is to say the difference between the size of the container and the size of the inner particle, has been identified as the design parameter that impacts most on maximum displacement reduction; its optimum value depends on the earthquake's characteristics. The results were confirmed for a primary structure with more degrees of freedom in [30, 31]. Reference [26] suggested adopting multiple VI NESs in conjunction with NESs having cubic nonlinearity for seismic mitigation. Another relevant design parameter of the VI NES, the particle-to-container mass ratio, is generally constrained by technological requirements and by the absorber's position over the primary structure, whereas the coefficient of restitution depends on the material properties and can be optimized under free vibrations [22].

The dynamics of the VI NES was studied experimentally and analytically in [36], wherein various vibrational regimes were observed. These regimes and their influence on the TET were accurately identified in [28, 38, 40]. Chaotic behavior was further analyzed through the analysis of the Lyapunov exponent in [38]. Energy dissipation due to impacts between multiple particles was investigated in [41, 42], while the technology and applications have been reviewed in [43, 44]. Recently, Ref. [45] proposed an experimental set-up made of a ceramic particle impacting on two oscillating rigid aluminium plates. A high-speed camera was employed to record the VI NES dynamics, and the particle motion was reconstructed with the aid of digital image correlation. This set-up allowed identifying the coefficients of restitution and friction forces. Since different orientations were tested, the effect of gravity was excluded. Still recently, a single contact vibro-impact damper has been coupled to the acoustic black hole effect for the passive vibration control of thin-walled structures [46, 47].

To the authors' knowledge, the contact dynamics was generally treated as an instantaneous phenomenon in previous researches on VI NES, including a phenomenological coefficient of restitution (COR). In contrast, the contact dynamics was considered in [46, 47] as an non-instantaneous but purely conservative phenomenon. Also, Ref. [45] adopted an ad-hoc Hertz-damped model based on an average interpenetration between colliding masses: here, an adjustment was made such that the trajectory of the particle obtained by means of video analysis matched the simulated one under harmonic loading. On the contrary, in the present study the particle is an inelastic sphere interacting with the inner walls according to the elasto-frictional Hertz-Mindlin potential, [48], including more realistic nonlinear viscoelastic dissipative contributions [49–51]. This allows improving the accuracy of the description of VI NES dynamics, and thus of its vibration absorption capability. In addition, our approach allows comparing side-by-side the finite duration and the instantaneous contact models, for close inspection within the scope of mechanical energy damping. Practically, in this paper

the VI NES, described by either a finite duration or an instantaneous contact model, is applied to the seismic control of a ten-story frame building, which is then benchmarked by considering two typical earthquakes in order to rule out specific effects.

The paper is organized as follows. The VI NES is presented in Section 2. Three contact models, namely an instantaneous description as a reference, in addition to *Tsuji* and *Kuwabara* viscoelastic interaction potentials as two possible variations of *Hertz* conservative repulsion, are introduced, again to rule out any specific features, to describe the interaction between the VI NES particle and the case walls. The equations of motion of an MDOF system (describing a benchmark ten-story building) coupled with a VI NES are then presented. In Section 3 the properties of the case study, consisting of a civil engineering benchmark frame building are presented. The influence of the initial conditions on the performance of the device, in term of energy dissipation, is then analyzed, by comparing results coming from the different contact models. Furthermore, the seismic responses of the overall system are shown and discussed. Finally, the conclusions are provided in Section 4.

2. Vibro-Impact Nonlinear Energy Sink

The VI NES studied here is similar to the device considered in [36–38], and its schematic representation is shown in Figure 1(a). Generally speaking, our VI NES is composed of a spherical particle enclosed within a hollow mass-spring-dashpot system. When the box oscillates, the sphere moves by rebounding against opposite edges. In the configuration considered here, the coupled system vibrates along the x-axis, which is perpendicular to the direction of gravity. When vibrated vertically, the particle bounces inside the container and takes-off when the acceleration of the container exceeds the gravity [42]. As in the previous research studies mentioned above, we made the choice to neglect the effect of the gravity and of the friction between the particle and the bottom surface, for the sake of clarity. Consequently, no rolling occurs and the VI NES has only one translational degree of freedom such that we can focus on collision dynamics only. In turn, we take into account the contact force and duration by implementing two viscoelastic dissipative contact models [49, 50]. There are two reasons for this. Firstly, it has been proven that Targeted Energy Transfer (TET) strongly depends on the VI NES response regime, ranging from chaos to 1:1 resonance with two impacts per cycle [52, 53]. The latter is considered as the optimal condition for energy dissipation under harmonic excitation [37, 54]. As a consequence, a proper estimation of contact duration is needed in order to account for such a delay on the overall dynamics in the time domain, especially under random excitation [55]. Secondly, in the present case study, collisions occur between a particle composing the VI NES and a MDOF oscillator. The so-called impulse–momentum model relying on COR (see below) is based on instantaneous impacts between two perfectly rigid masses without any other external forces, so that momentum is exchanged between the colliding bodies only; this excludes any transfer of energy and momentum to underlying coupled and any non-conservative collisions between more than two bodies at once. For instance, the presence of an elastic restoring spring beneath an impacted body modifies the energy balance and generates an inaccuracy in the estimation of the energy loss prescribed by the COR, since

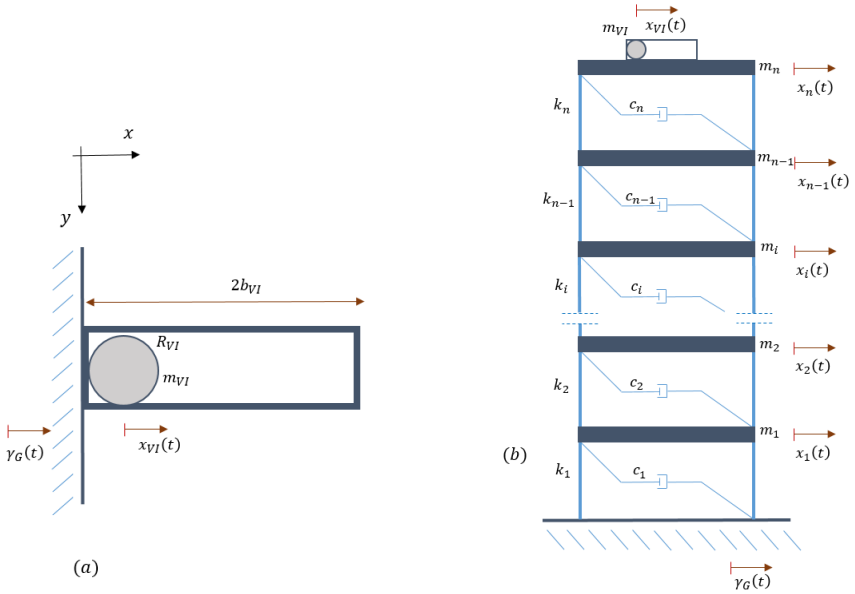

Figure 1: Schematic representation of (a) a VI NES and (b) a frame structure equipped with a VI NES on the top floor.

this secondary system is not taken into account in the model.

In Section 2.1, the theoretical models for elastic and viscoelastic contact are presented for the case of a ball bouncing between two fixed plates. Particular attention will be paid to the effect of finite contact duration on the system's dynamics and on the estimation of the energy transfer in a coupled system. In Section 2.2, the equations of motions of a MDOF system containing a VI NES will be presented.

2.1. Contact models

In contact mechanics, collisions between bodies can be regarded in the framework of the kinematics of either rigid or deformable bodies. In the case of rigid bodies, an instantaneous contact generates a change in direction of a particle free to move, with possibly some energy loss and velocity variation. In the case of deformable bodies, linear, nonlinear elastic, viscoelastic or plastic deformations may occur during contact. Accordingly, a contact force law has to be defined. Exhaustive literature reviews including pure elastic and dissipative contact force models were reported in [56, 57]. Taking into account the finite duration of the interaction and viscoelastic dissipation from a physical standpoint is a useful improvement with respect to previous research studies on VI NES. In the next subsections, the theoretical formulation of instantaneous and viscoelastic contact dynamics are detailed for the bouncing ball scheme. First, the basic principle governing instantaneous collisions between particles are recalled. Then, nonlinear elastic (*Hertz*) and viscoelastic (*Tsuji*, *Kuwabara*) models [49–51] are presented. The range of validity and accuracy of instantaneous and finite collisions are discussed.

2.1.1. Instantaneous collision

The normal collision between two particles, with mass $m_{1,2}$ and velocity $v_{1,2}(t)$, generates a repulsive force which conserves linear momentum even within a non-conservative interaction, $m_{1,2}\partial_t v_{1,2}(t) = \pm F(t)$, leading to

$$m_1 v_1(t_c) + m_2 v_2(t_c) = m_1 v_1(0) + m_2 v_2(0), \tag{1}$$

where $t = 0$ is the initial collision time and t_c stands for the contact duration. Nevertheless, the instantaneous collision case is obtained as the limit case for $t_c \approx 0$. According to the Newton's law of restitution [58], the relative velocity after impact is proportional and opposite in direction to the relative velocity before impact, resulting in:

$$\epsilon = \frac{v_1(t_c) - v_2(t_c)}{v_2(0) - v_1(0)}, \tag{2}$$

where $0 \leq \epsilon \leq 1$ is called the coefficient of restitution (COR). The COR is $\epsilon = 1$ in the case of conservative repulsion, and if the contact force is non-conservative, ϵ provides a measure of how much energy is dissipated during a binary collision, since it is possible to write:

$$K_r(t_c)/K_r(0) = \epsilon^2, \text{ where } K_r = \sum_{n=1}^{2} (1/2) m_n (v_n - v_{CM})^2 \text{ and } v_{CM} = \frac{\sum_{n=1}^{2} m_n v_n}{\sum_{n=1}^{2} m_n}, \tag{3}$$

K_r and v_{CM} being the relative kinetic energy and the velocity of the center of mass of the two particles, respectively. Now, by substituting Eq. 1 into Eq. 2 it is possible to determine the post-impact velocities:

$$v_1(t_c) = \frac{(m_1 - \epsilon m_2) v_1(0) + (m_2 + \epsilon m_2) v_2(0)}{m_1 + m_2}, \tag{4}$$

$$v_2(t_c) = \frac{(m_1 + \epsilon m_1) v_1(0) + (m_2 - \epsilon m_1) v_2(0)}{m_1 + m_2}. \tag{5}$$

The value of the coefficient of restitution ranges from $\epsilon = 0$ for perfectly inelastic collision to $\epsilon = 1$ for perfectly elastic collision [48]. It can be determined experimentally by dropping a particle from an initial height above an elastic surface and by measuring the rebound velocity [59]. The advantage of this scalar parameter is that it can be easily handled, but its precise value is not well referenced within standard databases of materials. Firstly, because it stands for a rough approximation of complex physics, and secondly because it is not an intrinsic feature of a material but results from the interaction between the two solids in contact.

The coefficient of restitution can also be determined from the measurement of the contact duration and the flight time of the particle between each bounce [60]. Generally, the contact duration t_c is very small when impacts occur between rigid bodies and is thus neglected, according to the instantaneous collision approximation. In this regard, Ref. [55]

experimentally validated an instantaneous collision model for a Single-Degree Of Freedom (SDOF) oscillator equipped with a vibro-impact damper composed by a steel particle and a fixed edge made of aluminum alloy. In the case study examined in [55], the contact time was found to be equal on average to 0.3 ms, which was considered sufficiently fast with respect to the natural period of the primary structure (0.25 s) to be neglected. However, in the Sec. 2.1.2 and later, we will show that accounting for a finite contact duration is in fact essential to make an accurate estimation of the energy dissipated by multiple impacts, even for a very fast contact duration. Moreover, the deceleration of the particles and consequently the repulsion force during the contact, predicted by the instantaneous contact model are flawed since $F \propto \partial_t v_{1,2} \simeq [v_{1,2}(t_c) - v_{1,2}(0)]/t_c$, see Eqs. 4 and 5: both arbitrarily tend to infinite when assuming $t_c \simeq 0$. On purpose, the finite duration collision models presented in the next section handle all these concerns.

2.1.2. Finite duration collision

i. Hertz model

According to the Hertzian interaction potential [48], the contact force F is

$$F(t) = C[\delta(t)]_+^{3/2}, \tag{6}$$

where δ is the overlap penetration between solids and $[\dots]_+$ denotes the Heavyside function, which relies on the absence of tensile force when the solids are not in contact. The prefactor C depends on the material properties and on the local radius of curvature near the contact area of the two bodies,

$$C = (4/3)E\sqrt{R}, \tag{7}$$

and is defined in terms of a reduced elastic modulus E and a reduced radius R, both defined as:

$$E = [(1-\nu_1^2)/E_1 + (1-\nu_2^2)/E_2]^{-1} \quad \text{and} \quad R = (R_1^{-1} + R_2^{-1})^{-1}, \tag{8}$$

where ν_1 and ν_2 and E_1 and E_2 are the Poisson's ratios and the Young's moduli of the two materials, respectively, and R_1 and R_2 are the local radii of curvature of the two bodies near the contact zone.

The contact duration t_c can be estimated by applying the principle of conservation of energy, considering that the incident kinetic energy of two colliding particles has to be converted first into the elastic deformation of the contact region, before bouncing back. At the maximal deformation, when the particles stop deforming, the initial kinetic energy $K = (1/2)mv^2$ is fully stored in potential energy $U = \int F d\delta = (2/5)C\delta^{5/2}$, where v is the relative contact velocity and $m = (m_1^{-1} + m_2^{-1})^{-1}$ is the reduced mass. Equalizing K and U leads to $\rho R^3 v^2 \propto ER^{1/2}(vt_c)^{5/2}$, by approximating the deformation rate as $v \propto \delta/t_c$ and considering ρ as the mass density of the materials composing the bodies. Hence, by introducing the elastic wave speed in the bulk material of the particle, $c_w \propto \sqrt{E/\rho}$, and by

introducing the elastic wave time-of-flight inside the particle $t_w \propto R/c_w$, one obtains

$$t_c \propto t_w (c_w/v)^{1/5} \propto t_w (R/\delta)^{1/4}. \tag{9}$$

It follows that $t_c \gg t_w$ at equilibrium, since $\delta \ll R$ and $v \ll c_w$, which pinpoints the quasi-static approximation [48] the Hertz potential relies on. Additionally, the scaling given in Eq. 9 demonstrates that the contact duration t_c can be safely neglected, as for instance in the instantaneous description, only if one also neglects the time t_w taken for an elastic deformation to propagate through an elastic body. The latter may result in inconsistencies, the elasticity being taken into account on the one hand but neglected on the other hand. Moreover, bearing in mind that the position and the velocity of interacting bodies can change very rapidly, a small error on the collision or rebound instant can lead to a noticeable bias on the exact relative velocities, and consequently on the transfers of energy and momentum, as demonstrated in Sec. 2.1.3.

In this study, we aim at using a VI NES to control the vibrations of a primary system, so the dissipative features of the contact law used for modeling impacts are crucial. To this end, we present in the next subsection two viscoelastic models, namely the *Tsuji* and the *Kuwabara* models. The former is fully relevant to the instantaneous model since it depends on the coefficient of restitution, but suffers from certain limitations which will be highlighted next. The latter introduces dissipation with a viscous relaxation time: this second finite duration model is provided as a direct comparison to *Tsuji*'s model, in order to rule out any of their specific features and help identify generic conclusions. In addition, it provides more reliable estimations of the dissipated energy in most situations (multibody collisions, collisions involving elastic systems) since it does not depend on a binary COR.

ii. Tsuji model

Here, we enrich the VI NES model by introducing the viscoelastic contact law proposed in [50]. The contact force between the two particles previously introduced is evaluated as the sum of an elastic Hertzian repulsion and a dissipative term proportional to the indentation rate $\partial_t \delta$

$$F(t) = C[\delta(t)]_+^{3/2} + D\sqrt{Cm}[\delta(t)]_+^{1/4}\partial_t\delta(t), \tag{10}$$

where m is the reduced mass, and the prefactor D depends only on ϵ according to [51],

$$D(\epsilon) = \frac{-\sqrt{5}\ln(\epsilon)}{\sqrt{\ln^2(\epsilon) + \pi^2}}. \tag{11}$$

It is noteworthy that the instantaneous contact model given in Eq. 2 to 5, and the *Tsuji* model given in Eqs. 10 and 11, both fit for a collision between two masses only. These models neither fit for a collision between more than two bodies nor for a collision between a particle and a more complex elastic system (for instance a mass-spring element), as it occurs for a VI NES coupled to a frame structure. Indeed, in these cases part of the momentum and energy is leaked to external bodies, so that instantaneous contact and *Tsuji* model can

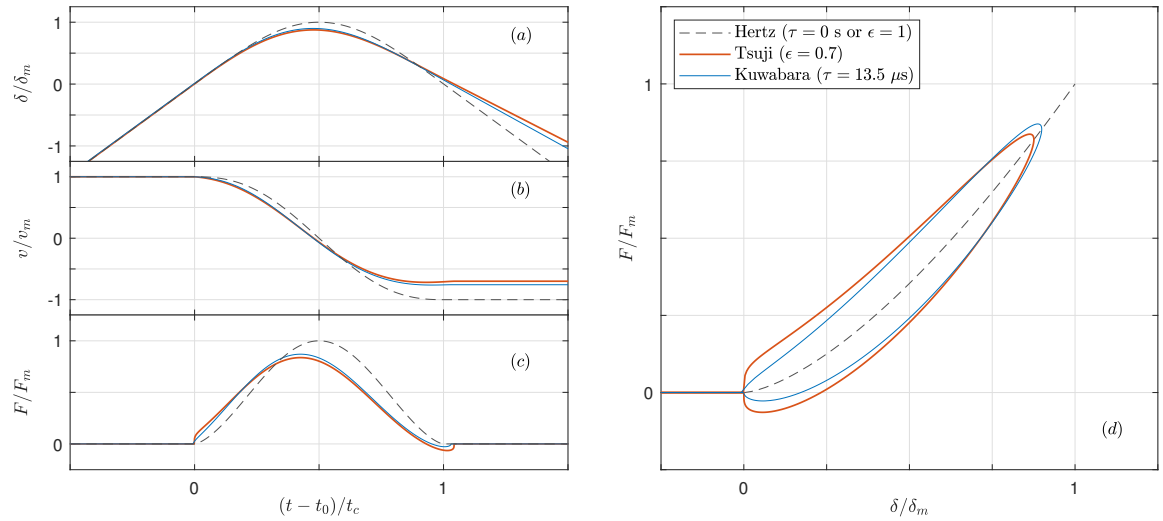

Figure 2: Contact between a steel particle of radius of 5 cm and a fixed plate. The initial velocity is $v_m = 1$ m/s. (a) Overlap deformation $\delta = (x - x_{plate})$, (b) deformation rate $v = \partial_t \delta$ and (c) repulsive force F of the contact as a function of time. (d) shows the force as a function of the deformation; the area within the curve is the dissipated energy. t_0 is the time of contact. The extrema δ_m and F_m and the contact duration t_c used to normalize all the curves refer to $\epsilon = 1.0$.

provide unexpected/unpredicted energy dissipation values. To overcome this drawback, we introduce a model which accounts for a dissipation mechanism at the contact level only, namely the *Kuwabara* model.

iii. Kuwabara model

The description proposed by Kuwabara and Kono in [49] accounts for a viscous relaxation time τ relying on a Kelvin-Voigt material approximation. The relaxation results in a delay between the force and the deformation, hence $F(t) = C[\delta(t+\tau)]_+^{3/2}$. Assuming weak dissipation, $\omega\tau \ll 1$ where $\omega \propto 1/t_c$ stands for the typical frequency content of a collision (i.e. $\tau \ll t_c$), and using a first order Taylor expansion over time, one recovers the ansatz given in [49]:

$$F(t) \simeq C[\delta(t)]_+^{3/2} + (3/2)\tau[\delta(t)]_+^{1/2}\partial_t\delta(t). \tag{12}$$

The formulation given in Eq. 12 has been proven to be physically relevant [56, 59, 61]. It requires only the knowledge of the intrinsic relaxation time of the materials composing the solids in contact. This information is readily available for most materials, like for example steel, in terms of loss angle ϕ_{loss} or loss factor $\eta_{loss} = \tan(\phi_{loss}) = \omega\tau$, where $\omega \propto 1/t_c$ is given by Eq. 9.

Practically, in the context of the present study it is possible to take advantage of the *Tsuji* model to relate τ and ϵ. Indeed, the comparison of Eq. 10 and Eq. 12 shows that the non-conservative term in *Tsuji*'s approximation qualitatively results in a nonlinear relaxation time $\tau \propto \sqrt{m/C}(D/\delta^{1/4}) \propto (DR/c_w)(R/\delta)^{1/4}$, such that $\eta_{loss} = \omega\tau \propto D(\epsilon)$. This estimation

tells that, in *Tsuji* model, the ratio of the dissipated to the stored energy during a collision only depends on the coefficient of restitution, and consequently do not depend on either the strength or the rate of the resulting deformation. Hence, it is possible to estimate *Kuwabara*'s relaxation time as

$$\tau \propto t_c(v) \times D(\epsilon) \tag{13}$$

from the knowledge of a nominal collision velocity v (see Eq. 9) and a coefficient of restitution ϵ. In other words, fulfilling Eq. 13 ensures that the dissipated energy per unit of stored energy (i.e. the loss factor) can be made the same for both *Tsuji* and *Kuwabara* models, for the sake of close comparison.

In order to demonstrate the equivalence of *Tsuji* and *Kuwabara* model, and their differences, we consider as an example in Fig. 2, a spherical particle of 5 cm radius thrown at an initial velocity of 1 m/s against an infinitely rigid and fixed wall. The particle is made of steel (mass density $\rho = 8000$ kg/m^3, Young's modulus 210 GPa and Poisson's ratio 0.3) and the coefficient of restitution is set to an arbitrary value $\epsilon = 0.7$. In Fig. 2, these two non-conservative models are compared to the conservative case of a *Hertzian* elastic model ($\epsilon = 1.0$, i.e. $\tau = 0$). Here, both *Kuwabara* and *Tsuji* contact models rely on the same magnitude of the non-conservative force, see Eqs. 10 and 12 within $v_m = 1$ m/s according to the protocol described in Eq. 13: this requires setting a relaxation time $\tau = 13.5$ μs for the former. Even within purely conservative mechanisms, the contact duration is finite due to the balance between inertia and elasticity. When viscoelasticity is taken into account, both the contact force and the maximal indentation become smaller and delayed between one and the other, see Fig. 2(a,c). The dissipated energy is represented by the area within the force-deformation loop, see Fig. 2(d). In Fig. 2(a,b) the particle displacement and velocity are shown. Owing to the similarities and differences of the non-conservative mechanical responses, we choose to perform the case study presented in Sec. 3 using both *Tsuji* and *Kuwabara* models. In all the cases considered in the following, we arbitrarily choose *Tsuji*'s COR at $\epsilon = 0.7$ and we then adjust the *Kuwabara*'s relaxtion time according to the protocol described in Eq. 13, for the sake of close comparisons.

2.1.3. Instantaneous versus finite duration collision

In this subsection, we provide an example, see Fig. 3, showing that a contact dynamics with finite duration has to be taken into account to obtain representative results even when the contact duration is small compared to the period of oscillation of a primary system, $t_c \ll T_1$. Such a requirement is even stronger when considering high eigenmodes (high frequency) of the primary system or soft/heavy particles (long contact duration, see Eq. 9). In addition, when considering the interaction between a particle damper and a resonant system (see Section 3), the finite duration ensures that a sudden change of direction at a rebound does not generate infinite deceleration and force, as it occurs with an instantaneous collision.

For the sake of side-by-side inspection, we compare here the instantaneous contact model given in Eq. 2 to 5 to *Tsuji* and *Kuwabara*'s finite duration contact models given in Eqs. 10

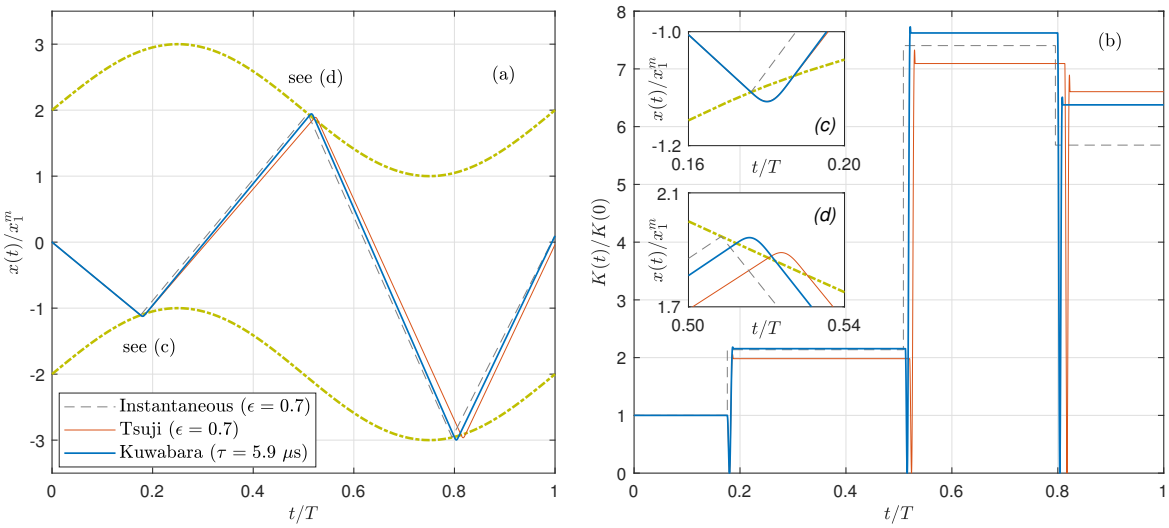

Figure 3: Simulated motion of the VI NES shown in Fig. 1(a). The VI NES is a steel sphere of radius 5 cm, enclosed in a rigid cylinder of width $b = 40$ cm and diameter 10 cm, and shaken kinematically at $f = 1/T = 100$ Hz with an amplitude $x_1^m = 10$ cm (see the green dashed curves). The initial velocity is $v_m = -62.8$ m/s. For the sake of clarity, the particle is considered as a point mass interacting with the inner walls of the container. (a) Position and (b) kinetic energy of the particle, according to instantaneous (black dashed line, see Eqs. 4-5) and finite duration contact dynamics evaluated according to Tsuji (red solid line, see Eqs. 10 and 11) and Kuwabara (blue solid line, see Eq. 12) model for $\epsilon = 0.7$.

and Eq. 12, respectively, which both rely on the coefficient of restitution ϵ, see Eq. 13. Here, no underlying mechanical system interacts with the colliding masses, the displacement of the container being forced kinematically: the instantaneous model and *Tsuji* model thus remain reliable and fully correspond to *Kuwabara* model according to Sec. 2.1.2-iii. These three models are compared in Figure 3. It can be seen that the first rebound introduces a delay between instantaneous and finite duration models, which makes the second collision and the later ones occur with different relative velocities. This leads to noticeably different energy transfer from one to the other, and thus of energy dissipation, even within a single period of oscillation, see insets (a) and (b). Here it is worth mentioning that the slight overshoot on the kinetic energy, predicted by finite contact models, relies on the brief attraction seen in Fig. 2 (see the negative force) which in turn is a well-known consequence of the viscoelastic-like delay between stress and strain, [51]. Interestingly, even a hardly noticeable differences between *Tsuji* and *Kuwabara* models at the first impact, see inset (c), generate different collision instant, and thus different dissipation level, as soon as the second impact occurs. It is thus essential to resolve the contact dynamics, even if the contact duration appears negligible compared to the period of oscillation. At this stage, one can see that none of the three models predict the same energy after only a single period of oscillation. However, it is worth noting that both finite contact duration models converge to the same final kinetic energy, $K(t = T) \simeq 6.48 \times K(t = 0)$, within a 1.5% relative difference, whereas the instantaneous model is off, $K(t = T) \simeq 5.68 \times K(t = 0)$, by about 12.5% this value.

This suggests that major improvement comes from main effect relies on taking into account for the finite duration of the *Hertzian* elastic contact, see Eq. 6. Here, the effect of the dissipative models, namely *Tsuji* or *Kuwabara*, remains marginal because the relaxation time they introduce is likely negligible compared to the conservative contact duration $\tau \ll t_c$. It turns out that whatever the finite contact duration model, an important requirement is that the non-conservative contribution dissipates the correct amount of energy, the correction on the contact duration remaining negligible if the dissipation can be considered weak.

2.2. Equations of motion of MDOF system coupled with a VI NES

In this Section, the equations of motion of a system composed by a MDOF linear system enclosing a VI NES are presented. A schematic representation of the arrangement considered is depicted in Figure 1(b). First, let us consider the equations of motion of a linear MDOF system, representing a n-DOF primary structure.

$$[\mathbf{M}]\,\partial_{tt}\{\mathbf{x}\} + [\mathbf{C}]\,\partial_{t}\{\mathbf{x}\} + [\mathbf{K}]\{\mathbf{x}\} = \{\mathbf{F}\}\,, \tag{14}$$

where $\{\mathbf{x}\} = \{x_1(t), x_2(t), \cdots, x_n(t)\}^T$ is the displacement vector. In the case of n mass-spring-dashpot oscillators arranged in series as shown in Figure 1(b), the mass $[\mathbf{M}]$, the damping $[\mathbf{C}]$ and the stiffness $[\mathbf{K}]$ matrices in Eq. 14 are given by:

$$[\mathbf{M}] = \begin{bmatrix} m_1 & 0 & \cdots & & 0 \\ 0 & m_2 & & & \\ \vdots & & \ddots & & \vdots \\ & & & m_{n-1} & 0 \\ 0 & & \cdots & 0 & m_n \end{bmatrix}, \quad [\mathbf{C}] = \begin{bmatrix} c_1+c_2 & -c_2 & 0 & \cdots & 0 \\ -c_2 & c_2+c_3 & -c_3 & 0 & \vdots \\ 0 & -c_3 & \ddots & & 0 \\ \vdots & 0 & & c_{n-1}+c_n & -c_n \\ 0 & \cdots & 0 & -c_n & c_n \end{bmatrix},$$
$$[\mathbf{K}] = \begin{bmatrix} k_1+k_2 & -k_2 & 0 & \cdots & 0 \\ -k_2 & k_2+k_3 & -k_3 & 0 & \vdots \\ 0 & -k_3 & \ddots & & 0 \\ \vdots & 0 & & k_{n-1}+k_n & -k_n \\ 0 & \cdots & 0 & -k_n & k_n, \end{bmatrix} \tag{15}$$

where m_i, c_i and k_i are the mass, the damping coefficient and the stiffness of the i-th oscillator for $i = 1, ..., n$.

The forces $\{\mathbf{F}\} = \{F_1(t), F_2(t), \cdots, F_n(t)\}^T$ acting on the MDOF system as it is defined in Eq. 14, depend on whether the reference frame is Galilean or not. If the reference is Galilean, the forces are ordinary external actions, and $\{\mathbf{x}\}$ represent the absolute displacements of the structure. On the contrary, in the case of seismic dynamics, one can consider Eq. 14 in the non-inertial reference frame of the oscillating ground, without external actions. In this situation, the resulting forces in Eq. 14 correspond to inertia forces, $F_i(t) = -m_i\gamma_G(t)$, where $\gamma_G(t) = \partial_{tt}x_G(t)$ stands for the absolute acceleration of the ground. In this case, $\{\mathbf{x}\}$

represent the motion of the structure relative to the moving reference [62].

Furthermore, when a VI NES is attached to the n-th oscillator, the equations of motion become:

$$[\mathbf{M}_{VI}]\,\partial_{tt}\{\mathbf{x}_{VI}\} + [\mathbf{C}_{VI}]\,\partial_t\{\mathbf{x}_{VI}\} + [\mathbf{K}_{VI}]\{\mathbf{x}_{VI}\} = \{\mathbf{F}_{VI}\}\,, \tag{16}$$

where

$$[\mathbf{M}_{VI}] = \begin{bmatrix}\mathbf{M} & \mathbf{0}\\ \mathbf{0} & m_{VI}\end{bmatrix},\quad [\mathbf{C}_{VI}] = \begin{bmatrix}\mathbf{C} & \mathbf{0}\\ \mathbf{0} & 0\end{bmatrix},\quad [\mathbf{K}_{VI}] = \begin{bmatrix}\mathbf{K} & \mathbf{0}\\ \mathbf{0} & 0\end{bmatrix}, \tag{17}$$

$\{\mathbf{x}_{VI}\} = \{\mathbf{x}(t), x_{VI}(t)\}^T$ and $\{\mathbf{F}_{VI}\} = \{\mathbf{F}\}^T + \{\mathbf{0}, F_c, -F_c\}^T$ (where $\mathbf{0}$ is a vector of size $n-1$).

It is noteworthy that $\{\mathbf{F}_{VI}\}$ is a nonlinear vector which depends explicitly on time, via the forcing $\{\mathbf{F}(t)\}$, and on the position and velocity of the Degree Of Freedom (DOF) via the contact force $F_c(x_{VI}, x_n, \partial_t x_{VI}, \partial_t x_n)$ acting between the VI NES and the upper DOF on which it stands, see for instance Eq. 10 or Eq. 12. In particular, F_c has no tensile contribution if the solids do not touch, so that $F_c\left[x_n(t) - x_{VI}(t) < R_{VI} - b_{VI}\right] = F\left[x_{VI}(t) < x_n(t) + b_{VI} - R_{VI}\right] = 0$, see Fig. 1(a). Otherwise, a compressive force occurs when the bodies come into contact, inducing loss through non-conservative repulsion between them, according to Eq. 10 or Eq. 12.

The system of Eqs. 16 can be made non-dimensional by normalizing the forces by the magnitude $F_1 = m_1 \max\{|\gamma_G(t)|\}$ the displacements by $x_1 = F_1/k_1$ and the time by the natural frequency of the undamped lowest DOF of the primary system, $\omega_1 = \sqrt{k_1/m_1}$. By introducing the dimensionless displacement $X_i = x_i/x_1$ and the dimensionless time $\theta = \omega_1 t$, Eq. 16 becomes:

$$\partial_{\theta\theta}\{\mathbf{X}_{VI}\} + [\boldsymbol{\zeta}_{VI}]\,\partial_\theta\{\mathbf{X}_{VI}\} + [\boldsymbol{\kappa}_{VI}]\{\mathbf{X}_{VI}\} = \{\boldsymbol{\gamma}_{VI}\}\,, \tag{18}$$

where $[\boldsymbol{\zeta}_{VI}] = [\mathbf{M}_{VI}]^{-1}[\mathbf{C}_{VI}]/\omega_1$, $[\boldsymbol{\kappa}_{VI}] = [\mathbf{M}_{VI}]^{-1}[\mathbf{K}_{VI}]/\omega_1^2$ and $\{\boldsymbol{\gamma}_{VI}\} = (m_1/F_1)$ $[\mathbf{M}_{VI}]^{-1}\{\mathbf{F}_{VI}\}$. By also introducing the non-dimensional velocity $\{\mathbf{V}_{VI}\} = \partial_\theta\{\mathbf{X}_{VI}\}$, the dynamical system can be written in a state space form.

$$\frac{\partial}{\partial\theta}\begin{Bmatrix}\mathbf{X}_{VI}(\theta)\\ \mathbf{V}_{VI}(\theta)\end{Bmatrix} = \begin{bmatrix}\mathbf{0} & \mathbf{I}\\ -\boldsymbol{\kappa}_{VI} & -\boldsymbol{\zeta}_{VI}\end{bmatrix}\begin{Bmatrix}\mathbf{X}_{VI}(\theta)\\ \mathbf{V}_{VI}(\theta)\end{Bmatrix} + \begin{Bmatrix}\mathbf{0}\\ \boldsymbol{\gamma}_{VI}(\mathbf{X}_{VI}, \mathbf{V}_{VI}, \theta)\end{Bmatrix}. \tag{19}$$

The latter system of nonlinear differential equations gives rise to a stiff problem since two different time scales are involved in the system dynamics, one originating from on the eigenvalues ω_i of the primary system, and the other, faster, from the contact duration, with $\omega_i \ll 1/t_c$. It is noteworthy that handling stiff problems requires a careful management of the numerical tolerances and convergences. Here, we have chosen to perform the numerical integration by using a generic Runge-Kutta numerical scheme at the order 4 with an adaptive time step (MATLAB's ode45) with a 10^{-4} relative tolerance and zero absolute tolerance, at the cost of slow and heavy calculations but gaining a robust management on how the energy conservation is fulfilled. Decreasing the relative tolerance to 10^{-5} produced results without

Story	1	2	3	4	5	6	7	8	9	10
Mass (t)	179	170	161	152	143	134	125	116	107	98
Inter-story stiffness (MN/m)	62.47	52.26	56.14	53.02	49.91	46.79	43.67	40.55	37.43	34.31
Normalized first mode shape	0.175	0.355	0.534	0.708	0.871	1.019	1.146	1.248	1.321	1.359

Table 1: Mass, stiffness and normalized first mode of the ten-story shear-type frame examined.

noticeable differences.

When dealing with the instantaneous model, the numerical simulations have been performed by parts, following an event driven scheme. An elementary simulation corresponds to the decoupled integration of the free flight of the particle in parallel to the dynamics of the MDOF given by Eq. (14): it terminates when the particle collides with a the other wall. The next simulation restarts right after the collision, with IC given by the positions and velocities of all the DOF at the end of the last run, just before the impact, but updated according to Eqs. 4 and 5. Such a scheme thus takes into account analytically for the interaction between the particle and the container. Following simulations are repeated until the seismic excitation ceases.

3. Passive control of a multi-story structure

3.1. Definition of case studies: benchmark building and seismic events

To assess the models presented in Sec. 2, numerical experiments were performed on a benchmark building endowed with a VI NES as seismic protection device. In particular, we consider the same ten-story shear-type frame structure first proposed in [63] to test a Tuned Mass Dampers for the passive control against seismic excitations; this building was examined for the same purpose in other studies, e.g., [64, 65].

The mass and inter-story stiffness properties of the structure considered are reported in Table 1. According to [64], the damping matrix $\mathbf{C}$ is assumed to be proportional to the stiffness matrix $\mathbf{K}$, with $\mathbf{C} = \tau_{is}\mathbf{K}$ and $\tau_{is} = 0.0129$ s. Regarding the modal properties, the first mode of vibration (fundamental and lowest frequency mode) is characterized by a frequency of 0.5072 Hz and by a damping ratio of 2.06 %, with a participating mass over 80 %. The normalized mode shape of the first mode of vibration is also reported in Table 1.

As seismic excitation, we choose two well-known historic ground motions, El Centro NS (1940) and Kobe NISHI-AKASHI (1995). El Centro NS signal (1940) seismic event is characterized by a relatively long ground motion duration, a relatively small value of peak ground acceleration (PGA) and a Fourier spectrum prominent in the range $0 - 2$ Hz, see Figure 4(a,b). On the other hand, Kobe NISHI-AKASHI (1995) shows a shorter duration and a large amount of energy around a narrow peak, see Figure 4(c,d). Here, the time axis of Kobe NISHI-AKASHI has been stretched in order to get its spectrum centered on the $0 - 2$ Hz frequency bandwidth, similar to El Centro NS: hereafter it will referred to as Kobe NA (1995 - scaled).

In Sec. 3.2, the VI NES will be designed according to each earthquake, in view of obtaining a significant seismic control of the ten-story shear-type frame examined in terms of

energy reduction. It is worth noting that our design strategy is not an optimization, but only lies in choosing the parameters providing a measurable response of an ordinary VI NES, in view of differentiating the few models to describe it. The sensitivity of the seismic control capacity of the VI NES regarding variations of the initial conditions, in terms of initial displacements and/or initial velocity of the particle, and regarding instantaneous versus finite duration contact models, will be also explored through a large number of numerical experiments.

3.2. Design of the test-bench VI NES

Many studies exist in the literature on design criteria regarding the optimal configuration of a VI NES in seismic application. Such a problem is a complex task because a nonlinear device like the VI NES may show high sensitivity to parameter variations. Here, a parametric study must be performed to identify reliable, but not necessarily optimal, values of the parameters governing the VI NES dynamics. In the literature on the seismic protection of civil structures, the effectiveness of a seismic device is generally expressed in terms of reducing the absolute or inter-story displacements, the acceleration or the energy injected into the structure, which is directly related to the stress level (elastic energy), or even all of these parameters together [66–69]. Here, we report the results of minimizing the cumulative elastic energy alone, that is the portion of the energy injected by the earthquake in the

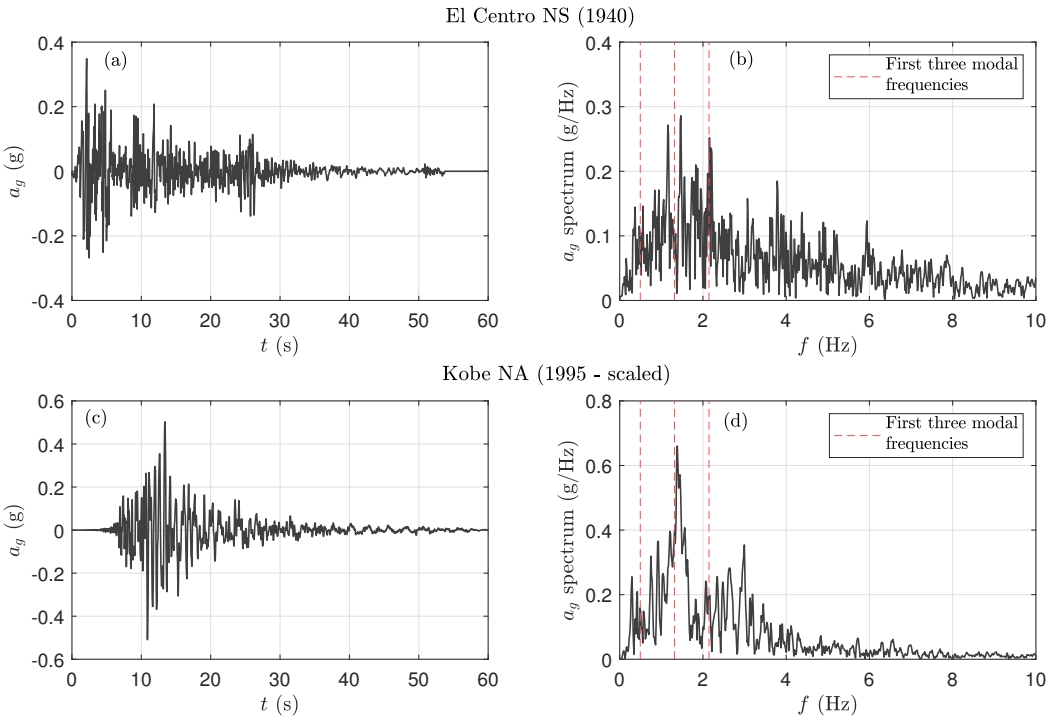

Figure 4: El Centro NS (1940) earthquake: (a) time history and (b) amplitude of the Fourier spectrum. Kobe NA (1995 - scaled) earthquake: (c) time history and (d) amplitude of the Fourier spectrum.

structure and converted into elastic deformation of the structural members of the frame. During an earthquake, the highest value of the acceleration usually occurs within a short time, after which a marked reduction of the excitation takes place. The reduction of the elastic energy thus gives a measure of the overall capability of the seismic device in controlling structural motions excited by the earthquake, whereas the maximum displacement of the top floor is directly linked to the maximum level of the internal stresses. The latter is essential for assessing if the structure will collapse or not during the seismic event considered, depending on its strength characteristics. Therefore, results obtained for the VI NES in terms of maximum displacement, inter-story drift and acceleration will be also presented in the next Section 3.3, for the sake of completeness.

Regarding the design of VI NES, we chose to fix one of its relevant parameters, that is the particle mass ($m_{VI} = 55.97$ t). This corresponds to a mass ratio of 5 % evaluated with respect to the modal mass of the first mode. Moreover, we consider arbitrarily that the box and the particle are made of steel (mass density $\rho = 8000$ kg/m^3, Young's modulus 210 GPa and Poisson's ratio 0.3). The above assumptions considerably simplify the design of the VI NES, since the only parameter to be determined is the clearance, represented by the dimensionless parameter $\beta = b_{VI}/R_{VI}$, with b_{VI} being the half-length of the box and R_{VI} the radius of the sphere, see Fig. 1(a), the latter being considered assigned once the mass and the material of the particle are fixed. Regarding the discussion in Sec. 2, the energy loss during the contacts can be represented either by instantaneous, *Tsuji* or *Kuwabara* models. For the sake of side-by-side comparisons, the same COR ϵ is arbitrarily assigned to the two formers, and by following the procedure described in Sec. 2.1.2-iii, the *Kuwabara*'s relaxation time τ is set such that it produces the same velocity dependent COR at a typical velocity explored by the system; here, we consider the typical velocity of the top floor, estimated as the pseudo-velocity S_{pv} of a SDOF oscillator at the natural frequency 0.5072 Hz (first mode of the frame structure) and considering a 2 % damping, that is $S_{pv} = 0.68$ m/s (El Centro NS) and $S_{pv} = 0.99$ m/s (Kobe NA, scaled).

The VI NES performance is represented by the energy reduction ratio E_r given by

$$E_r = \frac{E_e^{w/o}(t_{end}) - E_e^{VI}(t_{end})}{E_e^{w/o}(t_{end})}. \tag{20}$$

In Eq. 20, $E_e^{w/o}(t_{end})$ and $E_e^{VI}(t_{end})$ are the cumulative elastic energy in the uncontrolled structure and in the structure controlled by the VI NES, respectively, due to the earthquakes. The values are evaluated by referring to the whole duration, from $t = 0$ to $t = t_{end}$, of the time history records shown in Fig. 4. Here, the cumulative elastic energy of the building is the sum of the cumulative energies of each of its elastic contributions, $E_e = \sum_{i=1}^{10} E_{i,e}$ with $E_{i,e} = \int k_{s,i} x_{is,i} dx_{is,i}$, and $x_{is,i} = x_i - x_{i-1}$ for $i > 1$ and $x_{is,1} = x_1$.

As a first example, one considers the case of zero initial conditions, that is, the particle is at rest and in contact with the left wall of the box at the beginning of the seismic signal. The main results of the parametric study on β are summarized in Fig. 5 (dashed line with unfilled markers). For both ground motions, the effectiveness of the VI NES in reducing the

total elastic energy highly depends on β. Different contact models provide slightly different results, especially for high values of β. Fig. 5 depicts also the case of the particle in contact with the right wall at the beginning of the excitation (solid line with unfilled markers). As it can be seen, for the same β value, the energy reduction significantly depends on the initial position of the particle. This is particularly evident when the primary structure is subjected to El Centro NS (1940).

At this stage, studying in more details the sensitivity of seismic protection performances to the variation of the initial conditions (in terms of initial displacement and/or initial velocity of the particle) thus appears as a crucial aspect when selecting VI NES parameters and contact modeling. Such sensitivity to IC stems from the high nonlinearity of the VI NES, likely leading to chaotic behaviors. Actually, it is for instance not possible to exclude in advance that the effectiveness of the device might be substantially lowered if an earthquake occurs when the particle is at rest but is neither in contact with box's walls, nor it has zero velocity due to a forerunner earthquake motion. To assess the sensitivity of the VI NES with the ICs, a systematic campaign of numerical experiments was performed. In more details, the ICs in terms of displacement are varied across 11 values within the range $[0, 2b_{VI}]$ and the ICs in terms of velocity are varied across 21 values within the range $\left[-\max\{|v_{10}^{w/o}|\}, \max\{|v_{10}^{w/o}|\}\right]$, where $\max\{|v_{10}^{w/o}|\}$ is the maximum velocity of the 10-th floor determined for a reference IC (primary structure at rest) without any control device. Overall this represents more than two hundred different realizations of ICs.

The results of the sensitivity analysis described above are summarized in Fig. 5 (solid line with filled markers), which presents average values and standard deviations, of the reduction ratio E_r obtained by varying the ICs. One can clearly see first that the VI NES is sensitive to the ICs but the optimum β remains quite robust. From a more detailed analysis, three considerations can be made concerning the effect of the contact duration on the energy reduction. First, *Tsuji* and *Kuwabara* exhibit a similar trend, with standard deviation increasing identically for large values of β. Second, the VI NES modeled by an instantaneous contact results to be more sensitive to ICs, with high standard deviations all over the range of β. Third, all the three models provide similar trends, in average, for both seismic excitations. This allow us to conclude that, in this case study, the contact duration, finite or null, has little influence on the overall absorbed energy only if a large phase space is explored in terms of particle's initial conditions. In turn, for *Tsuji* and *Kuwabara*, the fact that the standard deviation is small means that only one or very few realizations yet provide reliable results in terms of E_r and β. Oppositely, the instantaneous model needs to be averaged over a larger set of realizations before converging to a reliable mean value: a single realization is clearly insufficient.

Here, the time responses of the finite contact models lowpass filters the dynamics of the system, see below in Sec. 3.3, and thus acts as a self-averaging process regularizing the mechanical response of the VI NES.

Summaries of the energy reduction for the two earthquakes are reported in Table 2 (El Centro NS) and Table 3 (Kobe NA, scaled). In particular, the VI NES provides an average elastic energy reduction of 60.8 % $\leq E_r \leq$ 63.8 % for $\beta = 1.25$ under El Centro NS, and

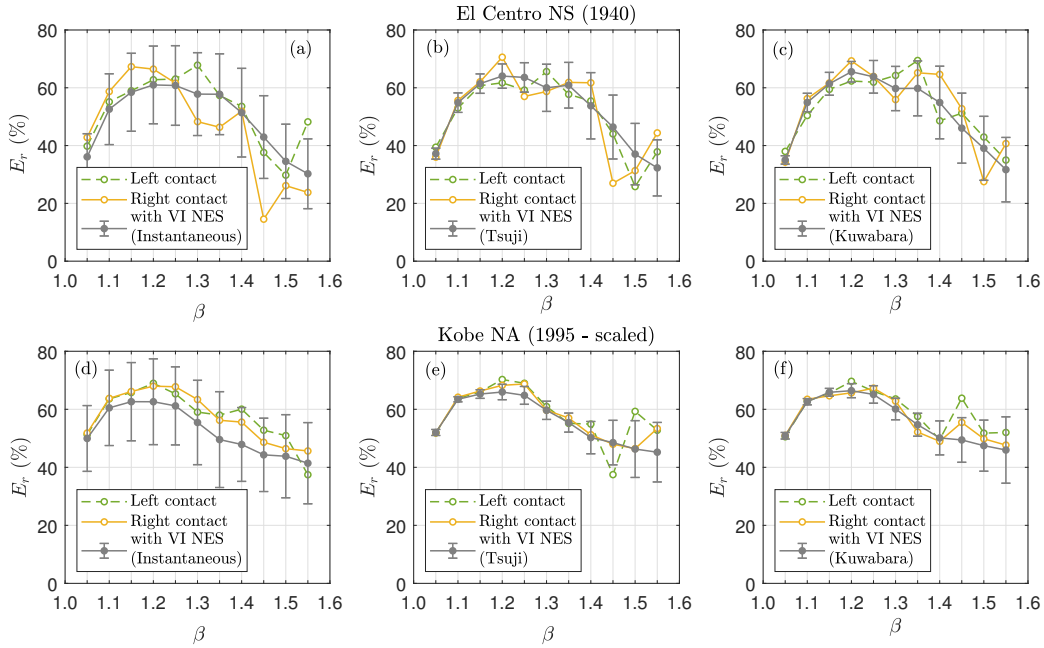

Figure 5: Parametric study on the effectiveness of the VI NES in controlling the structure in terms of reduction of the cumulative elastic energy (see Eq. 20). Primary structure is subjected to (a,b,c) El Centro NS (1940) and (d,e,f) Kobe NA (1995 - scaled) ground motion. The VI NES is modeled according to (a,d) Instantaneous, (b,e) *Tsuji* and (c,f) *Kuwabara* contact. Average value and standard deviations are calculated from 11×21 different ICs. For left and right contact ICs are $x_{0,VI} = R_{VI} - b_{VI}$, $v_{0,VI} = 0$, and $x_{0,VI} = b_{VI} - R_{VI}$, $v_{0,VI} = 0$, respectively. Solid line with filled markers stands for average, vertical lines stand for $\pm\sigma_{VI}$.

62.6 % $\leq E_r \leq$ 66.4 % $\beta = 1.2$ under Kobe NA scaled. These two values of β provide in average the higher elastic energy reduction.

Here, we recover a result derived by Sack et al. [70], demonstrating that it exists a clearance β maximizing the dissipated energy in a vibrated granular media enclosed in a box, which essentially depends on the displacement amplitude of the vibration. The strength of our two earthquakes being different, see Fig 4, we chose the value $\beta = 1.25$ for the case of El Centro NS and $\beta = 1.2$ for the case of Kobe NA scaled earthquakes, respectively, for determining the length of the box of the VI NES. These values provide a significant effect on the seismic response for the purpose of comparing models with respect to the modal features of the structure and to the spectral features of the earthquakes considered. Such design may however not correspond to a more global optimum per se, which is beyond the scope of this study. Comparing both earthquakes while noticing that they have approximately the same peak amplitude, one can infer that the optimal β, 1.2 versus 1.25, is somehow independent of the time or frequency details of the seismic excitations. In contrast, arbitrarily rescaling the magnitude of an earthquake by $\pm$25% (results not shown) revealed that the optimal β weakly changes by about $\pm$10%: the larger the amplitude, the larger the value of β. Table 4 summarizes the main parameters characterizing the VI NESs.

El Centro NS (1940)	**Left contact**	**Right contact**	**Average**	σ
Instantaneous	63.0 %	61.6 %	60.8 %	13.8 %
Tsuji	59.2 %	57.0 %	63.6 %	5.1 %
Kuwabara	61.9 %	63.9 %	63.8 %	5.6 %

Table 2: Performance sensitivity of the VI NES ($\beta = 1.25$) to ICs when the primary structure is subjected to El Centro NS (1940) time history and depending on contact duration. Left and right contact denotes results for the VI NES initially at rest and in contact with a wall of the structure. Average and standard deviations σ are calculated from 11×21 different ICs.

Kobe NA (1995-scaled)	**Left contact**	**Right contact**	**Average**	σ
Instantaneous	68.9 %	68.0 %	62.6 %	14.8 %
Tsuji	70.3 %	68.3 %	65.9 %	2.6 %
Kuwabara	69.6 %	65.7 %	66.4 %	2.4 %

Table 3: Performance sensitivity of VI NES ($\beta = 1.2$) to initial conditions when primary structure is subjected to Kobe NA (1995 - scaled) time history and depending on contact duration. Left and right contact denotes results for the VI NES initially at rest and in contact with a wall of the structure. Average and Standard deviations σ are calculated from 11×21 different initial conditions.

The effectiveness of the seismic protection of the VI NES will be discussed in Sec. 3.3, with a particular attention to the effects of the contact duration.

3.3. Seismic response and discussion

The seismic behavior of the ten-story shear-type frame considered under the two benchmark earthquakes is now discussed. The main features of the response are presented for the structure with and without the VI NES control device; in particular, the effect of the contact model is underlined. Seismic protection device has been designed with respect to the structure and the earthquake considered, according to the description given in Sections 3.1 and 3.2. As for the ICs, the particle of the VI NES is hereafter considered initially at rest in the middle of the box, i.e. $x_{0,VI} = 0$, $v_{0,VI} = 0$. Figures 6(a,b) represent the time history of the lateral displacement of the 10-th floor for the uncontrolled structure or for the structure controlled by the VI NES. First, it is clear that the VI NES induce a marked displacement mitigation especially during the first seconds of the earthquakes, i.e. during the time when maximum displacements occur, and therefore when the most severe stress states on the structure take place.

Still, Figs. 6(c,d) show the cumulative elastic energy for the uncontrolled structure and for the structure controlled by the VI NES. It can be readily seen that in the first 20

Earthquake	**Material**	ϵ	m_{VI} (t)	$2R$ (m)	$2b$ (m)
El Centro NS (1940)	Steel	0.7	55.79	2.37	2.96
Kobe NA (1995 - scaled)	Steel	0.7	55.79	2.37	2.84

Table 4: Properties of the VI NES designed for the ten-story shear-type frame structure subjected to El Centro NS (1940) and Kobe NA (1995 - scaled) earthquakes.

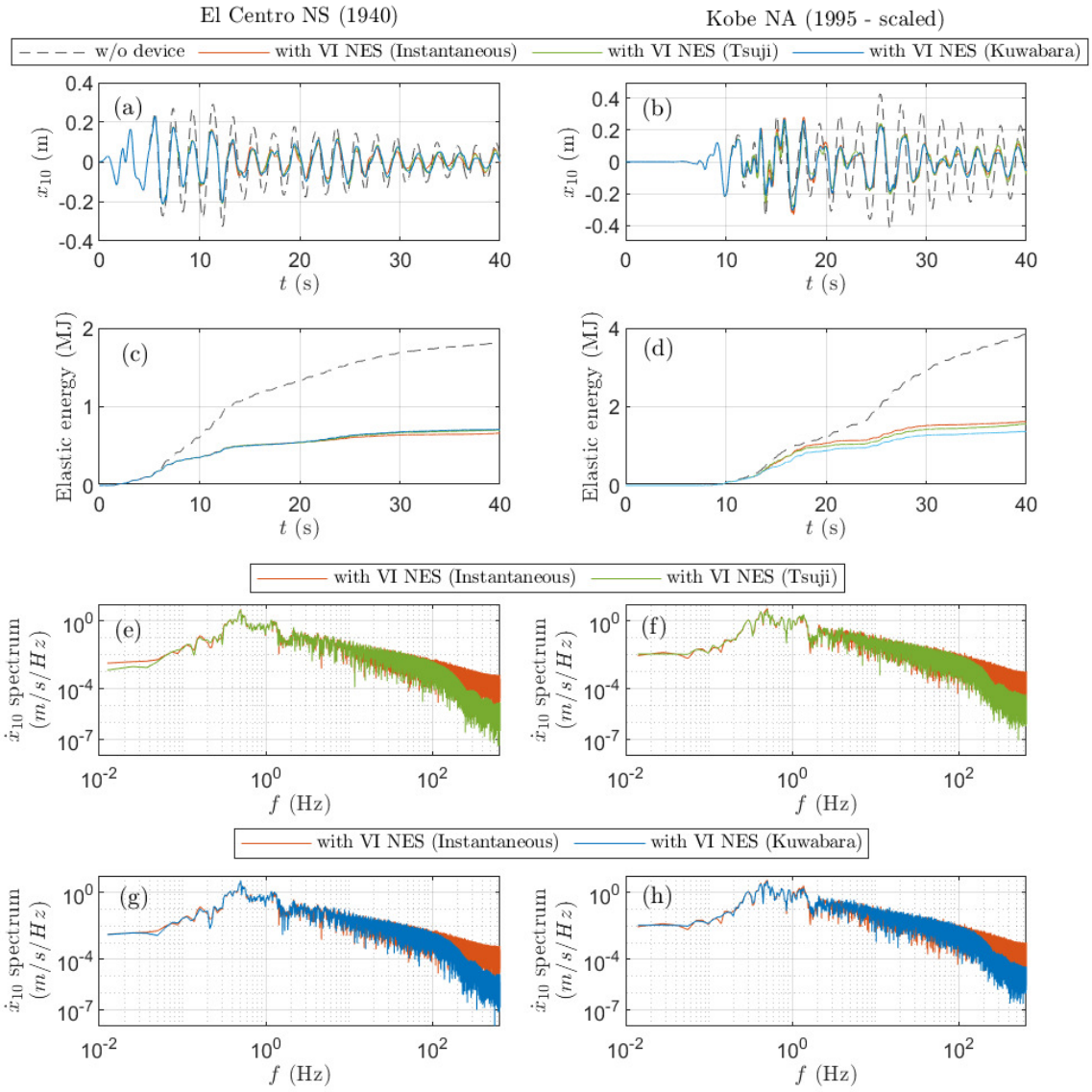

Figure 6: (a,b) Time history of the lateral displacement of the 10-th floor, (c,d) cumulative elastic energy for the uncontrolled structure and for the structure controlled by the VI NES and (e,f,g,h) Fourier spectrum amplitude of the 10-th floor velocity for the structure controlled by the VI NES. (a,c,e,g) $\beta = 1.25$, El Centro NS (1940). (b,d,f,h) $\beta = 1.2$, Kobe NA (1995 - scaled). For all cases ICs are $x_{0,VI} = 0$, $v_{0,VI} = 0$.

seconds of motion, when the seismic excitation is more intense, the VI NES yields the highest energy reduction. Slight discrepancies between estimations of the elastic energy arise from the features of the contact models employed and are more prominent under Kobe NA scaled time history. However, the dissimilarities cannot be attributed to the parametrization of the three models. Instantaneous and *Tsuji* models rely on the same COR, whereas *Kuwabara*'s relaxation time is set such that the contact duration is the same as *Tsuji* within a typical range of impact velocity v, see Eq. 13. Here, it is interesting to

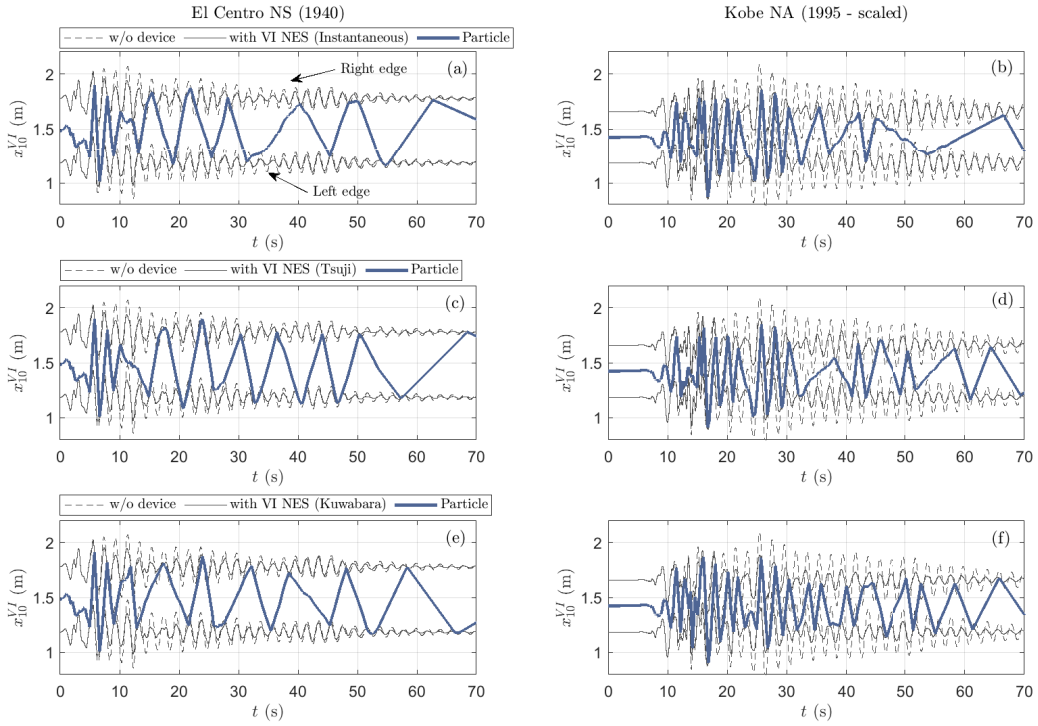

Figure 7: Time history of the displacement of the opposite walls and of the particle of VI NES for the uncontrolled structure and for the structure controlled by the VI NES with different contact models. (a,c,e) $\beta = 1.25$, El Centro NS (1940). (b,d,f) $\beta = 1.2$, Kobe NA (1995 - scaled). For all cases ICs are $x_{0,VI} = 0$, $v_{0,VI} = 0$.

remind that such typical velocity was assumed to range around the pseudo-velocity S_{pv} at the first modal frequency of the frame structure. In average over the first 30 seconds of both earthquakes, we check the reliability of this assumption since the impact velocities span over $\langle v \rangle = 0.60 \pm 0.45$ m/s versus $S_{pv} = 0.68$ m/s for El Centro NS, while it is $\langle v \rangle = 0.90 \pm 0.54$ m/s versus $S_{pv} = 0.99$ m/s for Kobe NA scaled.

Figures 6(e,f,g,h) show the Fourier spectrum amplitude of the 10-th floor velocity for the structure controlled by the VI NES. As it can be seen, instantaneous contact spreads some energy content to high frequencies, whereas *Tsuji* and *Kuwabara* act as low pass filters of the dynamics response of the system up to a cutoff frequency of the order of the inverse of the typical contact duration $\omega_c \propto 1/t_c$, avoiding the system to fall into nonphysical chaotic states.

In Figure 7, the time history of the displacement of the two opposite walls of the box and of the particle of the VI NES are represented for both El Centro NS and Kobe NA scaled ground motions. It is evident that the high efficiency of the VI NES in limiting the maximum displacements is linked to the fact that in the first instants, when the highest accelerations occur, the particle impacts both walls at each cycle of motion (two impacts per period of oscillation). This generates head-on collisions that impede the motion and hence

limit the amplitude of displacement. Afterwards, a diminution of the number of the impacts is observed, resulting in a decrease of the effectiveness in structural control. This dynamic is caught by all contact models. However, as expected, the estimated contact duration affects the exact history of the particle motion, the number and the time of impacts.

Finally, Figure 8 provides a more in-depth description of the effects of the VI NES in terms of controlling the structure under earthquake excitations: it represents the maximum relative displacements of each floor of the structure, Figs. 8(a,d), the maximum inter-story drifts relative to each story, Figs. 8(b,e), and the maximum accelerations of each floor, Figs. 8(c,f). It is interesting to note that the predictions given by the three models look very similar for El Centro NS earthquake, whereas significant differences appear under Kobe NA scaled excitation. This is due to the fact that the differences between models accumulate and thus increase with the number of impacts, consistently with the results seen in Fig. 3. Accordingly, looking into the details of the collision dynamics under both earthquakes reveals that the maximum displacement and inter-story drift are attained after no more than two impacts for El Centro NS, and after more than ten impacts for Kobe NA scaled, see Fig. 7. The satisfactory performance in terms of displacements of the VI NES stands out for each floor under both excitations. On the other hand, the top-floor acceleration and the inter-story drift are increased with respect to the uncontrolled case due to short impacts. In particular, the maximum acceleration of the last floor estimated by the instantaneous contact model is more than an order of magnitude larger than the one obtained with *Tsuji* or *Kuwabara* models. This is due to the fact that the instantaneous contact model asymptotically predicts infinite accelerations and contact forces, which are arbitrarily bounded in practice by the inverse of the numerical time step.

These results are consistent with previous studies, in particular with the fact that a VI NES can be used as seismic protection device, at least if one considers the performance in terms of maximum elastic energy and relative displacement reduction, a crucial aspect for avoiding structural collapse. Indeed, the results presented in Fig. 8 show a detrimental effect of the VI NES in the top floor inter-story drift and in the top floor maximum acceleration. Our analysis demonstrates that the simulation of such a system needs to be handled with care since the features at very different time scales influence one on the others. However, we show that the differences due to inaccurate estimations coming from approximations at the lowest order of contacts duration, such as for instance the instantaneous hypothesis, can be avoided by averaging over a large phase space of initial conditions. Here, finite contact duration models accelerate the convergence by reducing the number of needed realizations: contrarily to the instantaneous model, a single realization may somehow be sufficient to render an average trend.

4. Conclusion

The VI NES is a non-smooth nonlinear system and its dynamics is greatly affected by the impact velocity, contact duration and initial conditions. The analyses presented in this paper deepen the issue of the influence of the contact modeling strategy in describing the dynamics of a VI NES, here employed for the vibration control of a civil engineering frame

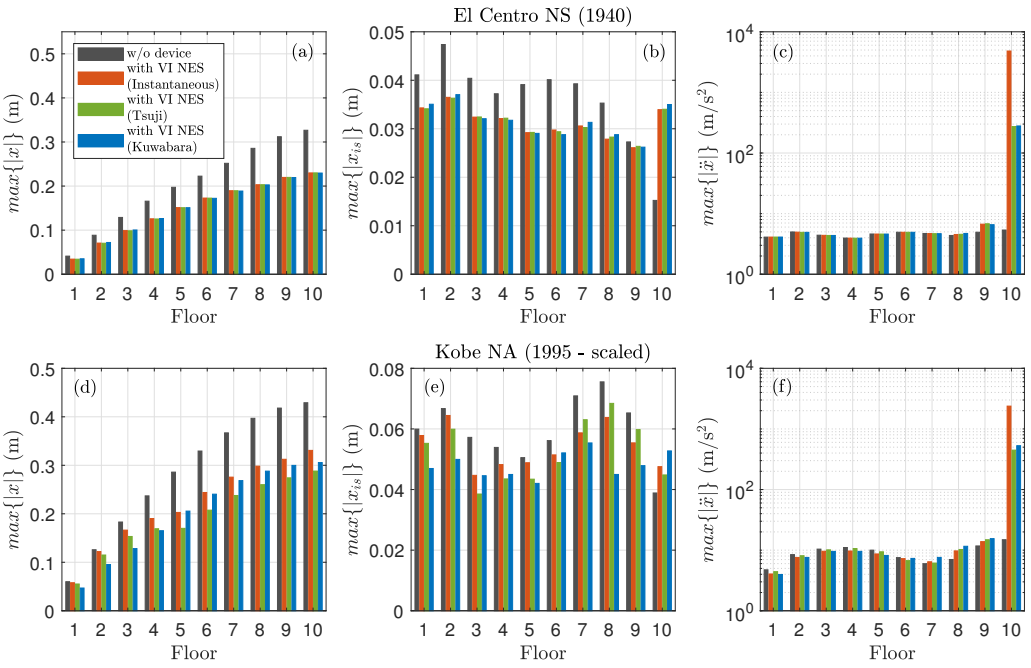

Figure 8: Seismic response at each floor of the frame structure for the uncontrolled structure, and for the structure controlled by the VI NES with different contact models. (a,b,c) $\beta = 1.25$, El Centro NS (1940). (d,e,f) $\beta = 1.2$, Kobe NA (1995 - scaled). ICs: $x_{0,VI} = 0$, $v_{0,VI} = 0$. (a,d) maximum displacement, $\max\{|x|\}$, (b,e) maximum inter-story drift, $\max\{|x_{is}|\}$ and (c,f) maximum acceleration, $\max\{|\partial_{tt}x|\}$.

structure under a seismic excitation. In addition to the instantaneous contact model, usually employed in the literature, finite duration contact models like *Tsuji* and *Kuwabara* models are considered. Specifically, *Tsuji* model can be seen as a finite duration evolution of the instantaneous model, since both make use of the concept of coefficient of restitution to quantify the dissipation. On the contrary, *Kuwabara* model introduces the dissipation with a relaxation time. These two models are made arbitrarily equivalent in terms of contact duration and losses, the aim being to compare them with the instantaneous approximation.

The examined case study is a ten story frame building endowed with a VI NES on the top floor. A sensitivity analysis on initial displacement and velocity of the VI NES particle highlighted the robustness of the VI NES against initial conditions in order to select a clearance. In addition, our results showed that finite duration contact models make the system less sensitive to the initial conditions in the sense that they are both characterized by smaller standard deviations, i.e. smaller fluctuations between a run with an IC and another. It turns out that fewer realizations lead to somehow reliable prediction in terms of suitable clearance and energy reduction.

The qualitative dynamic of the system is caught by all contact models: higher vibration absorption is achieved by the VI NES at the beginning of the earthquake, where nearly a 1:1 resonance between the primary structure and the particle occurrs; after, a diminution of the number of the impacts is observed, and therefore a diminution of the seismic control

capacity. The overall elastic energy reduction remains comparable for all cases due to the fact that the majority of the energy is absorbed in the first instants of motion. Anyway, the instantaneous contact approximation erroneously spreads part of the mechanical energy to incommensurately high frequencies, in contrast with *Tsuji* and *Kuwabara* models. The two latter finite duration contact models indeed act as low pass filters of the dynamics response of the system, avoiding the system to fall into nonphysical chaotic states.

From the quantitative point of view, the accelerations and the repulsive forces are greatly affected by the contact model employed, with values at the floor supporting the VI NES being incommensurately and arbitrarily large when considering the instantaneous approximation. This last shortcoming prevents the design of a practical system able to withstand the internal shocks, for instance.

Whether it is a high sensitivity to ICs, an incommensurately high frequency range or an incommensurately high amplitude of the mechanical response, all these features depend on the contact stiffness of the VI NES and on how carefully it is approximated and handled. In practice, one may accommodate these flaws by introducing soft elastic elements in addition to the VI NES, for instance like (i) a soft elastic spring in parallel to a mechanical stop or (ii) a soft bumper in series, on which the VI NES bounces. In the former case, the dynamics will be dictated by the stiff collisions, likely leading to similar observations and conclusions, as in our case study. In the latter case, the dynamics will be dictated by the softer element, leading to finite contact duration even within the instantaneous approximation; here finite contact models would become pointless. A third option would be to consider a container enclosing a particle and connected to the primary structure with a spring. This situation qualitatively relies on the present study (the container being in practice the 10-th floor itself). Here, the spring-mass system will filter and thus moderate the transmitted force and acceleration to the primary system, but the sensitivity to ICs would likely remain unchanged, as observed similarly in our case study; here, accurate predictions will benefit from the use of finite contact duration models.

In further developments, an experimental validation is likely to be useful and promising to test our findings. This aspect is actually under active developments, which in turn might require a more complete modeling in order to mimic a realistic system; one possible perspective is for instance to account for the lateral friction and rotational/rolling motion of the particle. Finally, an important outcome is to determine how robust is the VI NES when subjected to any arbitrary seismic signal. For this, an in-depth systematic analysis of random excitation signals using appropriate statistical techniques is needed.

CRediT

Stefania Lo Feudo: Conceptualization, Investigation, Methodology, Numerical simulations, Project administration, Writing. **Stéphane Job**: Conceptualization, Formal analysis, Investigation, Methodology, Numerical simulations, Writing. **Miriam Cavallo**: Investigation, Numerical simulations, Writing. **Aguinaldo Fraddosio**: Conceptualization, Investigation, Methodology, Writing. **Mario Daniele Piccioni**: Conceptualization,

Investigation, Methodology, Writing. **Alessandro Tafuni**: Investigation, Numerical simulations, Writing.

Acknowledgment

This research was partially supported by Erasmus+ programme of the European Union through Master's students mobility. We thank Anne-Laure Vialette (ISAE-ENSMA) and Antoine Faulconnier (Supméca Groupe ISAE) for their contribution given at the early stages of this study (Software).

Funding

This research did not receive any specific grant from funding agencies in the public, commercial, or not-for-profit sectors.

References

[1] F. Légeron, P. Paultre, J. Mazars, Damage mechanics modeling of nonlinear seismic behavior of concrete structures, Journal of Structural Engineering 131 (6) (2005) 946–955. doi:10.1061/(asce)0733-9445(2005)131:6(946).

[2] X. Ji, G. Fenves, K. Kajiwara, M. Nakashima, Seismic damage detection of a full-scale shaking table test structure, Journal of Structural Engineering 137 (1) (2011) 14–21. doi:10.1061/(asce)st.1943-541x.0000278.

[3] C. Ramirez, A. Liel, J. Mitrani-Reiser, C. Haselton, A. Spear, J. Steiner, G. Deierlein, E. Miranda, Expected earthquake damage and repair costs in reinforced concrete frame buildings, Earthquake Engineering and Structural Dynamics 41 (11) (2012) 1455–1475. doi:10.1002/eqe.2216.

[4] I. Koutromanos, A. Stavridis, P. Shing, K. William, Numerical modeling of masonry-infilled rc frames subjected to seismic loads, Computers and Structures 89 (11 - 12) (2011) 1026–1037. doi:10.1016/j.compstruc.2011.01.006.

[5] A. Stavridis, I. Koutromanos, P. Shing, Shake-table tests of a three-story reinforced concrete frame with masonry infill walls, Earthquake Engineering and Structural Dynamics 41 (6) (2012) 1089 – 1108. doi:10.1002/eqe.1174.

[6] H. Zhang, J. Kuang, T. Yuen, Low-seismic damage strategies for infilled rc frames: shake-table tests, Earthquake Engineering and Structural Dynamics 46 (14) (2017) 2419 – 2438. doi:10.1002/eqe.2911.

[7] A. F. Vakakis, O. Gendelman, Energy pumping in nonlinear mechanical oscillators, II: resonance capture, Journal of Applied Mechanics 68 (1) (2001) 42 – 48. doi:10.1115/1.1345525.

[8] A. F. Vakakis, O. V. Gendelman, L. A. Bergman, M. D. McFarland, G. Kerschen, Y. S. Lee, Nonlinear targeted energy transfer in mechanical and structural systems, Springer, New - York, 2008. doi:10.1007/978-1-4020-9130-8.

[9] E. Gourdon, N. A. Alexander, C. A. Taylor, C. H. Lamarque, S. Pernot, Nonlinear energy pumping under transient forcing with strongly nonlinear coupling: Theoretical and experimental results, Journal of Sound and Vibration 300 (3 - 5) (2007) 522–551. doi:10.1016/j.jsv.2006.06.074.

[10] H. Ding, L. Chen, Designs, analysis, and applications of nonlinear energy sinks, Nonlinear Dyn 100 (2020) 3061–3107. doi:10.1007/s11071-020-05724-1.

[11] P. O. Mattei, R. Ponçot, M. Pachebat, R. Côte, Nonlinear targeted energy transfer of two coupled cantilever beams coupled to a bistable light attachment, Journal of Sound and Vibration 373 (2016) 29–51. doi:10.1016/j.jsv.2016.03.008.

[12] S. Lo Feudo, C. Touzé, J. Boisson, G. Cumunel, Nonlinear magnetic vibration absorber for passive control of a multi–storey structure, Journal of Sound and Vibration 438 (2019) 33–53. doi:10.1016/j.jsv.2018.09.007.
[13] F. Romeo, L. I. Manevitch, L. A. Bergman, A. Vakakis, Transient and chaotic low-energy transfers in a system with bistable nonlinearity, Chaos: An Interdisciplinary Journal of Nonlinear Science 25 (5) (2015) 053109. doi:10.1063/1.4921193.
[14] D. Michael McFarland, L. A. Bergman, A. F. Vakakis, Experimental study of non-linear energy pumping occurring at a single fast frequency, Int. Journal of Non–linear Mechanics 40 (2005) 891–899. doi:10.1016/j.ijnonlinmec.2004.11.001.
[15] M. AL-Shudeifat, Highly efficient nonlinear energy sink, Nonlinear Dyn 76 (2014) 1905–1920. doi:10.1007/s11071-014-1256-x.
[16] P. Zhou, H. Li, Modeling and control performance of a negative stiffness damper for suppressing stay cable vibrations, Structural Control and Health Monitoring 23 (4) (2016) 764 – 782. doi:10.1002/stc.1809.
[17] Y. Chen, Z. Qian, K. Chen, P. Tan, S. Tesfamariam, Seismic performance of a nonlinear energy sink with negative stiffness and sliding friction, Structural Control and Health Monitoring 26 (2019) e2437. doi:10.1002/stc.2437.
[18] S. Benacchio, A. Malher, J. Boisson, C. Touzé, Design of a magnetic vibration absorber with tunable stiffnesses, Nonlinear Dynamics 85 (2016) 893–911. doi:10.1007/s11071-016-2731-3.
[19] G. Pennisi, B. P. Mann, N. Naclerio, C. Stephan, G. Michon, Design and experimental study of a nonlinear energy sink coupled to an electromagnetic energy harvester, Journal of Sound and Vibration 437 (2018) 340–357. doi:10.1016/j.jsv.2018.08.026.
[20] M. A. AL-Shudeifat, N. E. Wierschem, L. A. Bergman, A. F. Vakakis, Numerical and experimental investigations of a rotating nonlinear energy sink, Meccanica 52 (2017) 763–779. doi:10.1007/s11012-016-0422-2.
[21] X. Lu, Z. Liu, Z. Lu, Optimization design and experimental verification of track nonlinear energy sink for vibration control under seismic excitation, Structural Control and Health Monitoring 24 (12) (2017) e2033. doi:10.1002/stc.2033.
[22] M. A. AL-Shudeifat, A. Saeed, Comparison of a modified vibro-impact nonlinear energy sink with other kinds of NESs, Meccanica 56 (2021) 735–752. doi:10.1007/s11012-020-01193-3.
[23] A. Saeed, M. A. AL-Shudeifat, A. Vakakis, et al., Rotary-impact nonlinear energy sink for shock mitigation: analytical and numerical investigations, Arch Appl Mech 90 (2020) 495–521. doi:10.1007/s00419-019-01622-0.
[24] J. Wang, N. E. Wierschem, B. Wang, B. F. Spencer Jr, Multi-objective design and performance investigation of a high-rise building with track nonlinear energy sinks, The Structural Design of Tall and Special Buildings 29 (2) (2020) e1692. doi:10.1002/tal.1692.
[25] M. A. AL-Shudeifat, N. Wierschem, D. D. Quinn, A. F. Vakakis, L. A. Bergman, B. F. Spencer, Numerical and experimental investigation of a highly effective single-sided vibro-impact non-linear energy sink for shock mitigation, International Journal of Non-Linear Mechanics 52 (2013) 96–109. doi:10.1016/j.ijnonlinmec.2013.02.004.
[26] J. Luo, N. E. Wierschem, S. A. Hubbard, L. A. Fahnestock, D. Dane Quinn, D. Michael McFarland, B. F. Spencer, A. F. Vakakis, L. Bergman, Large-scale experimental evaluation and numerical simulation of a system of nonlinear energy sinks for seismic mitigation, Engineering Structures 77 (2014) 34–48. doi:10.1016/j.engstruct.2014.07.020.
[27] I. Karayannis, A. F. Vakakis, F. Georgiades, Vibro-impact attachments as shock absorbers, Proceedings of the Institution of Mechanical Engineers, Part C: Journal of Mechanical Engineering Science 222 (10) (2008) 1899–1908. doi:10.1243/09544062JMES864.
[28] O. Gendelman, A. Alloni, Dynamics of forced system with vibro-impact energy sink, Journal of Sound and Vibration 358 (2015) 301 – 314. doi:10.1016/j.jsv.2015.08.020.
[29] W. Li, N. Wierschem, X. L. et al., Numerical study of a symmetric single-sided vibro-impact nonlinear energy sink for rapid response reduction of a cantilever beam, Nonlinear Dyn 100 (2020) 951–971.

doi:10.1007/s11071-020-05571-0.
[30] F. Nucera, F. Lo Iacono, D. Michael McFarland, L. Bergman, A. Vakakis, Application of broadband nonlinear targeted energy transfers for seismic mitigation of a shear frame: Experimental results, Journal of Sound and Vibration 313 (1) (2008) 57–76. doi:10.1016/j.jsv.2007.11.018.
[31] F. Nucera, D. Michael McFarland, L. Bergman, A. Vakakis, Application of broadband nonlinear targeted energy transfers for seismic mitigation of a shear frame: Computational results, Journal of Sound and Vibration 329 (15) (2010) 2973–2994. doi:10.1016/j.jsv.2010.01.020.
[32] M. Ahmadi, N. K. A. Attari, M. Shahrouzi, Structural seismic response mitigation using optimized vibro-impact nonlinear energy sinks, Journal of Earthquake Engineering 19 (2) (2015) 193–219. doi:10.1080/13632469.2014.962671.
[33] A. Arena, W. Lacarbonara, A. Casalotti, Payload oscillations control in harbor cranes via semi-active vibration absorbers: modeling, simulations and experimental results, Procedia Engineering 199 (2017) 501–509, x International Conference on Structural Dynamics, EURODYN 2017. doi:10.1016/j.proeng.2017.09.136.
[34] G. Stefani, M. D. Angelis, U. Andreaus, Scenarios in the experimental response of a vibro-impact single-degree-of-freedom system and numerical simulations, Nonlinear Dyn 103 (2021) 3465–3488. doi:10.1007/s11071-020-05791-4.
[35] M. A. AL-Shudeifat, Nonlinear Energy Sinks With Piecewise-Linear Nonlinearities, Journal of Computational and Nonlinear Dynamics 14 (12) (10 2019). doi:10.1115/1.4045052.
[36] G. Pennisi, C. Stephan, E. Gourc, G. Michon, Experimental investigation and analytical description of a vibro-impact NES coupled to a single–degree–of–freedom linear oscillator harmonically forced, Nonlinear Dynamics 88 (3) (2017) 1769–1784. doi:10.1007/s11071-017-3344-1.
[37] T. Li, S. Seguy, A. Berlioz, On the dynamics around target energy transfer for vibro–impact nonlinear energy sink, Nonlinear Dynamics 87 (2017) 1453 – 1466. doi:10.1007/s11071-016-3127-0.
[38] T. Li, C. Lamarque, S. Seguy, A. Berlioz, Chaotic characteristic of a linear oscillator coupled with vibro–impact nonlinear energy sink, Nonlinear Dynamics 91 (4) (2018) 2319 – 2330. doi:10.1007/s11071-017-4015-y.
[39] F. Nucera, A. Vakakis, D. Michael McFarland, L. Bergman, G. Kerschen, Targeted energy transfers in vibro-impact oscillators for seismic mitigation, Nonlinear Dyn 50 (2007) 651–677. doi:10.1007/s11071-006-9189-7.
[40] Y. S. Lee, F. Nucera, A. F. Vakakis, D. Michael McFarland, L. A. Bergman, Periodic orbits, damped transitions and targeted energy transfers in oscillators with vibro-impact attachments, Physica D: Nonlinear Phenomena 238 (18) (2009) 1868–1896. doi:10.1016/j.physd.2009.06.013.
[41] F. Pacheco-Vázquez, S. Dorbolo, Rebound of a confined granular material: combination of a bouncing ball and a granular damper, Scientific Reports 3 (1) (jul 2013). doi:10.1038/srep02158.
[42] M. Masmoudi, S. Job, M. Abbes, I. Tawfiq, M. Haddar, Experimental and numerical investigations of dissipation mechanisms in particle dampers, Granular Matter 18 (2016) 71. doi:10.1007/s10035-016-0667-4.
[43] Z. Lu, Z. Wang, S. Masri, X. Lu, Particle impact dampers: Past, present, and future, Structural Control and Health Monitoring 25 (2018) e2058. doi:10.1002/stc.2058.
[44] Z. Lu, F. Masri, X. Lu, Particle Damping Technology Based Structural Control, Springer Tracts in Civil Engineering, Springer Singapore, 2020. doi:10.1007/978-981-15-3499-7.
[45] R. Chabrier, E. Sadoulet-Reboul, G. Chevallier, E. Foltête, T. Jeannin, Full-field measurements with digital image correlation for vibro-impact characterisation, Mechanical Systems and Signal Processing 156 (2021) 107658. doi:10.1016/j.ymssp.2021.107658.
[46] H. Li, C. Touzé, A. Pelat, F. Gautier, X. Kong, A vibro-impact acoustic black hole for passive damping of flexural beam vibrations, Journal of Sound and Vibration 450 (2019) 28–46. doi:10.1016/j.jsv.2019.03.004.
[47] H. Li, C. Touzé, A. Pelat, F. Gautier, Combining nonlinear vibration absorbers and the acoustic black hole for passive broadband flexural vibration mitigation, International Journal of Non-Linear Mechanics (2020) 103558doi:10.1016/j.ijnonlinmec.2020.103558.

[48] K. L. Johnson, Contact Mechanics, Cambridge University Press, 1985. doi:10.1017/CBO9781139171731.
[49] G. Kuwabara, K. Kono, Restitution coefficient in a collision between two spheres, Japanese Journal of Applied Physics 26 (8) (1987) 1230–1233. doi:10.1143/jjap.26.1230.
[50] Y.Tsuji, T. Tanaka, T. Ishida, Lagrangian numerical simulation of plug flow of cohesionless particles in a horizontal pipe, Powder Technology 71 (3) (1992) 239–250. doi:10.1016/0032-5910(92)88030-l.
[51] D. Antypov, J. A. Elliott, On an analytical solution for the damped hertzian spring, EPL (Europhysics Letters) 94 (5) (2011) 50004. doi:10.1209/0295-5075/94/50004.
[52] E. Gourc, G. Michon, S. Séguy, A. Berlioz, Targeted energy transfer under harmonic forcing with a vibro-impact nonlinear energy sink: Analytical and experimental developments, Journal of Vibration and Acoustics 137 (3) (2015) 031008. doi:10.1115/1.4029285.
[53] T. Li, E. Gourc, S. Seguy, A. Berlioz, Dynamics of two vibro-impact nonlinear energy sinks in parallel under periodic and transient excitations, International Journal of Non-Linear Mechanics 90 (2017) 100–110. doi:10.1016/j.ijnonlinmec.2017.01.010.
[54] D. Qiu, S. Seguy, M. Paredes, Design criteria for optimally tuned vibro-impact nonlinear energy sink, Journal of Sound and Vibration 442 (2019) 497–513. doi:10.1016/j.jsv.2018.11.021.
[55] K. Li, A. Darby, Modelling a buffered impact damper system using a spring-damper model of impact, Structural Control and Health Monitoring 16 (3) (2009) 287–302. doi:10.1002/stc.238.
[56] A. Stevens, C. Hrenya, Comparison of soft-sphere models to measurements of collision properties during normal impacts, Powder Technology 154 (2005) 99–109. doi:10.1016/j.powtec.2005.04.033.
[57] P. Flores, H. Lankarani, Contact Force Models for Multibody Dynamics, Vol. 226 of Solid Mechanics and its Applications, Springer, 2016. doi:10.1007/978-3-319-30897-5.
[58] I. Cook, Newton's 'experimental' law of impacts, The Mathematical Gazette 70 (452) (1986) 107. doi:10.2307/3615768.
[59] E. Falcon, C. Laroche, S. Fauve, C. Coste, Behavior of one inelastic ball bouncing repeatedly off the ground, The European Physical Journal B 3 (1998) 45–57. doi:10.1007/s100510050283.
[60] M. Nagurka, S. Huang, Mass–spring–damper model of a bouncing ball, International Journal of Engineering Education 22 (2) (2006) 393 – 401.
[61] S. Job, F. Melo, A. Sokolow, S. Sen, How hertzian solitary waves interact with boundaries in a 1d granular medium, Phys. Rev. Lett. 94 (2005) 178002. doi:10.1103/physrevlett.94.178002.
[62] A. K. Chopra, Dynamics of Structures, 5th Edition, 5th Edition, Pearson, 2017.
[63] F. Sadek, B. Mohraz, A. Taylor, R. Chung, A method of estimating the parameters of tuned mass dampers for seismic applications, Earthq Eng Struct Dyn 26 (6) (1997) 617–635. doi:10.1002/(sici)1096-9845(199706)26:6<617::aid-eqe664>3.0.co;2-z.
[64] M. Hadi, Y. Arfiadi, Optimum design of absorber for MDOF structures, Journal of Structural Engineering 124 (11) (1998) 1272 – 1280. doi:10.1061/(asce)0733-9445(1998)124:11(1272).
[65] S. Etedali, H. Rakhshani, Optimum design of tuned mass dampers using multi-objective cuckoo search for buildings under seismic excitations, Alexandria Engineering Journal 57 (4) (2018) 3205–3218. doi:10.1016/j.aej.2018.01.009.
[66] M. Chey, J. Chase, J. Mander, A. Carr, Semi-active tuned mass damper building systems: Design, Earthquake Engineering and Structural Dynamics 39 (2010) 119–139. doi:10.1002/eqe.934.
[67] D. Pietrosanti, M. D. Angelis, M. Basili, Optimal design and performance evaluation of systems with tuned mass damper inerter (tmdi), Earthquake Engineering and Structural Dynamics 46 (8) (2017) 1367–1388. doi:10.1002/eqe.2861.
[68] S. Elias, Seismic energy assessment of buildings with tuned vibration absorbers, Shock and Vibration 2018 (2018) 1–10. doi:10.1155/2018/2051687.
[69] M. Morales-Beltran, G. Turan, O. Dursun, R. Nijsse, Energy dissipation and performance assessment of double damped outriggers in tall buildings under strong earthquakes, Structural Design of Tall and Special Buildings 28 (1) (2019) e1554. doi:10.1002/tal.1554.
[70] A. Sack, M. Heckel, J. E. Kollmer, F. Zimber, T. Pöschel, Energy dissipation in driven granular matter in the absence of gravity, Phys. Rev. Lett. 111 (2013) 018001. doi:10.1103/PhysRevLett.111.018001.